MINIMALLY INVASIVE CLASSIFICATION OF PANCREATIC CYSTIC NEOPLASMS

Sharib J, Ivry S, Dominguez D, Hatcher S, Gilbert E, Kim G, Craik CS, Kirkwood KS.

Background: Pancreatic cyst detection is rising at an alarming rate. Our lab has previously shown that proteolytic activity in pancreatic cyst fluid can distinguish mucinous cysts from nonmucinous cysts, and as a result, can save many patients from unnecessary surveillance and surgery. We now hypothesize that cyst fluid proteolysis can be used to stratify pancreatic cystic neoplasms based on degree of dysplasia.
Methods: We characterized secreted proteolytic activity signatures in cyst fluid of 60 pancreatic cysts using multiplex substrate profiling by mass spectrometry (MSP-MS). Specific activity features associated with malignant cysts were used to develop classifiers for malignancy using statistical modeling. Distinguishing activity features served as the basis for fluorescent peptide substrates design that we have incorporated into a simple, activity assay for assessment of dysplasia using cyst fluid. Finally, a second blinded cohort of 120 cyst fluid samples will be used to validate our fluorescent assay for pathologic grade.

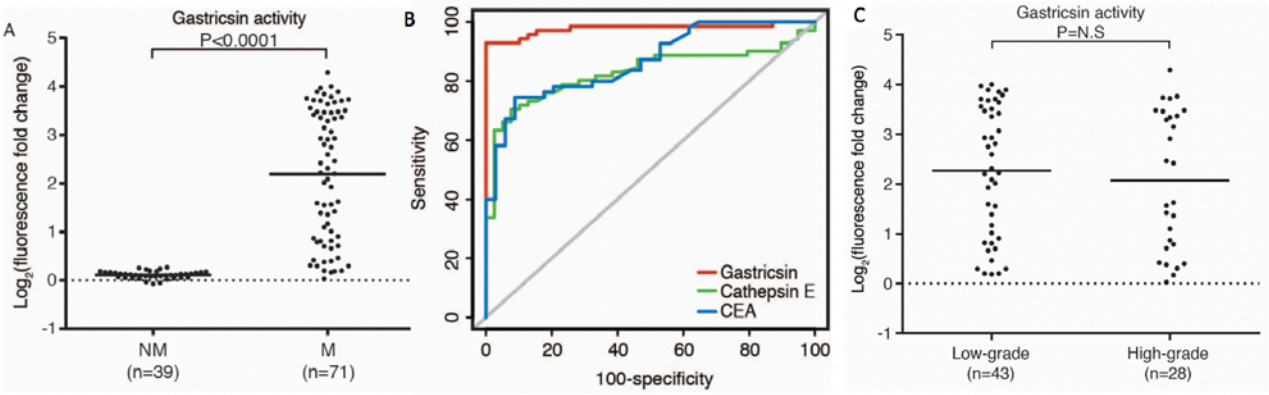

Fig 1. (A) Gastricsin differentiates mucinous cysts from nonmucinous cysts. **(B)** ROC curves for diagnosing mucinous cysts. **(C)** Gastricsin has modest ability to distinguish high grade dysplasia from low grade dysplasia in mucinous cysts.

Results: Two hundred cleavage events unique to malignant mucinous cysts were detected in a pilot cohort of fluid from 17 pancreatic cystic neoplasms. Quantification of proteolysis for several peptide substrates designed from the unique cleavages readily differentiated nonmucinous cysts from malignant mucinous cysts in the initial sample cohort. Two initial Förster resonance energy transfer (FRET) probes were synthesized to mimic peptide substrate sequences in the MSP-MS library. Proteomic analysis identified the aspartyl proteases, cathepsin E and gastricsin as the primary endoproteases against these substrates respectively. Analysis of 110 cyst fluid samples of varying type by the FRET probes showed clear distinction between mucinous and nonmucinous cysts (Fig 1a). The sensitivity and specificity for identifying mucinous cysts were 93% and 100% (ROC 0.98) with our gastricsin FRET assay, versus 64% and 94% (AUC 0.84) respectively for CEA, the current standard, applied to the same sample (Fig 1b). When comparing only mucinous cysts, the FRET assay was able to identify 14/28 cysts with high grade dysplasia (Fig 1c). While the probes were not able to differentiate grade in our limited cohort, we are exploring whether activity of the current or additional FRET peptide substrates can be used to identify high grade dysplasia in a larger, validation cohort.
Conclusion: Proteolysis is superior to the current gold standard, carcinoembryonic antigen (CEA), in distinguishing mucinous from nonmucinous pancreatic cysts. Use of this diagnostic will save patients from unnecessary surgery. Further discrimination between low and high grade dysplasia would spare many more patients the burdens of overtreatment.

Perivascular Delivery of Resolvin D1 Inhibits Inflammation and Neointimal Hyperplasia in a Rabbit Vein Graft Model

Evan Werlin, Bian Wu, Giorgio Mottola, Anuran Chatterjee, Mian Chen, Kevin D Lance, Dan A Bernards, Brian Sansbury, Matt Spite, Tejal A Desai, Michael S Conte

Introduction: The long-term success of interventions for peripheral arterial disease is limited by restenosis due to intimal hyperplasia, which we believe is caused by an aberrant, persistent inflammatory response. Specialized pro-resolving lipid mediators (SPM) such as resolvin D1 (RvD1), have been shown to counteract inflammation and promote the process of resolution. We investigate the effects of local perivascular delivery of RvD1 in a rabbit vein graft model.

Methods: Ipsilateral jugular veins were implanted as carotid interposition grafts via an anastomotic cuff technique in New Zealand white rabbits (3-4 kg; n=34). RvD1 was delivered (1mg) to the vein bypass grafts in a perivascular fashion via bi-layered biodegradable poly-lactic-co-glycolic acid (PLGA) wrap. Rabbits were sacrificed at either 3 or 28 days following bypass. Total leukocyte infiltration and macrophage infiltration were evaluated via immunohistochemistry (IHC) on grafts explanted on day 3. Cell proliferation was also evaluated via IHC on grafts explanted 3 and 28 days following bypass. Elastin staining was conducted on grafts harvested at 28 days post-bypass to evaluate neointimal hyperplasia (NIH).

Results: Perivascular application of RvD1-wraps was associated with a reduction in total leukocyte infiltration versus both bypass-only (246.8 vs 1133.0 cells per mm^2, $P < .01$) and vehicle-wrap groups (246.8 vs 766.1 cells per mm^2, $P < .01$). Rabbits treated with vehicle-wraps demonstrated reduced leukocyte infiltration compared to the bypass-only group (766.1 vs 1133.0 cells per mm^2, $P < .05$) but increased macrophage infiltration (545.4 vs 304.3 cells per mm^2, $P < .05$), suggesting a macrophage response to the device. Perivascular application of RvD1-wraps was associated with reduced cellular proliferation at 3 days versus the vehicle-wrap group (24% vs 41% cells per mm^2, $P < .05$) and demonstrated a trend towards decreased proliferation versus bypass only (24% vs 36%, $P = .105$). There were no significant differences in proliferation between groups at 28 days post-bypass (<1% across all groups). RvD1-wraps also significantly decreased neointimal formation when compared to the bypass-only group (56 μm vs 112 μm; $P < .001$), and there was a trend towards decreased neointimal formation when comparing the RvD1-wrap group to the vehicle-wrap (56 μm vs 82 μm, $P = .085$).

Conclusions: Local perivascular delivery of the pro-resolving lipid mediator RvD1 reduces neointimal hyperplasia following experimental vein grafting through a reduction of leukocyte recruitment and attenuated cell proliferation in the graft. Our study provides further support for the potential therapeutic role of SPM such as D-series resolvins in modulating vascular injury and repair.

Understanding the Biology of Cytotoxic T Lymphocytes in Human Cancer

Kelly M Mahuron, Priscila Munoz Sandoval, Mariela L Pauli, Evan Henley, Adil I Daud, Michael D Rosenblum

Introduction:
Inhibition of the PD-1 pathway has revolutionized the treatment of melanoma and other cancers, but only a minority of patients respond to treatment. We have previously demonstrated that the relative abundance of partially exhausted CD8+ cytotoxic T lymphocytes (peCTLs) expressing both the inhibitory receptors PD-1 and CTLA-4 within the tumor microenvironment correlates with response to anti-PD-1 monotherapy for metastatic melanoma. The aim of this study is to comprehensively phenotype these CTLA-4^{hi}PD-1^{hi} peCTLs through immune profiling and whole transcriptome RNA sequencing to better understand the fundamental biology of these cells. In addition, we will determine if these cells are found in cancers other than melanoma and whether they are predictive of clinical responses to anti-PD-1 therapy in these settings.

Methods:
Multiparameter flow cytometry was performed on freshly isolated tumor samples from patients with advanced cancer. In addition to quantifying levels of PD-1 and CTLA-4 expression on CD8 T cells, levels of other candidate markers were compared between the CTLA-4^{hi}PD-1^{hi} peCTL populations and the other CD8 T cells within the tumor microenvironment. Statistical analysis was performed with Prism v6 software and all P values were generated with paired t-tests.

Results:
To further define the peCTL population predictive of response to anti-PD-1 therapy, we set out to determine whether these cells have more of an effector-like or memory-like phenotype. Using multiparameter flow cytometry, multiple markers were analyzed on freshly isolated melanoma biopsies (Figure 1). Percentages of Ki-67, a cellular marker for proliferation and activation, were significantly higher in peCTLs compared to other CD8 T cells in the tumor microenvironment (**p=0.0012). Levels of memory-associated marker CD45RA, the chemokine receptor CCR7, and the IL-7 receptor CD127 were all significantly decreased in peCTLs (*p=0.010, *p=0.049, *p=0.002 respectively). This profile suggests that peCTLs are very active and have an″effector memory-like″ phenotype.

In ongoing studies, we will analyze the peCTL population through whole transcriptome RNA sequencing. To date, we have FACS purified the PD-1^{hi}CTLA-4^{hi} peCTL subset from 10 metastatic melanoma samples. We will compare and contrast the transcriptional profile of these cells to the profile of the other CD8 T cells found within the same tumors.
In addition, we have been analyzing cancers other than melanoma to determine if a similar peCTL subset can be observed within these tumors and if the presence of this population correlates with response to anti-PD-1 therapy. To date, we have demonstrated CTLA-4^{hi}PD-1^{hi} peCTL populations within tumors from Kaposi's Sarcoma, Merkel Cell Carcinoma, and Nasopharyngeal Carcinoma.

Conclusions:
Through comprehensive immune profiling, we have demonstrated that the peCTL population predictive of anti-PD-1 therapy response is highly activated and has an "effector memory-like" phenotype. By complementing this approach with whole transcriptome RNA sequencing, we plan to elucidate critical pathways involved in the generation, maintenance, and activation of this immune cell subset. A better understanding of the fundamental biology of these cells will provide a foundation for novel therapeutic approaches aimed at augmenting the tumor intrinsic immune system to fight cancer.

Figure 1

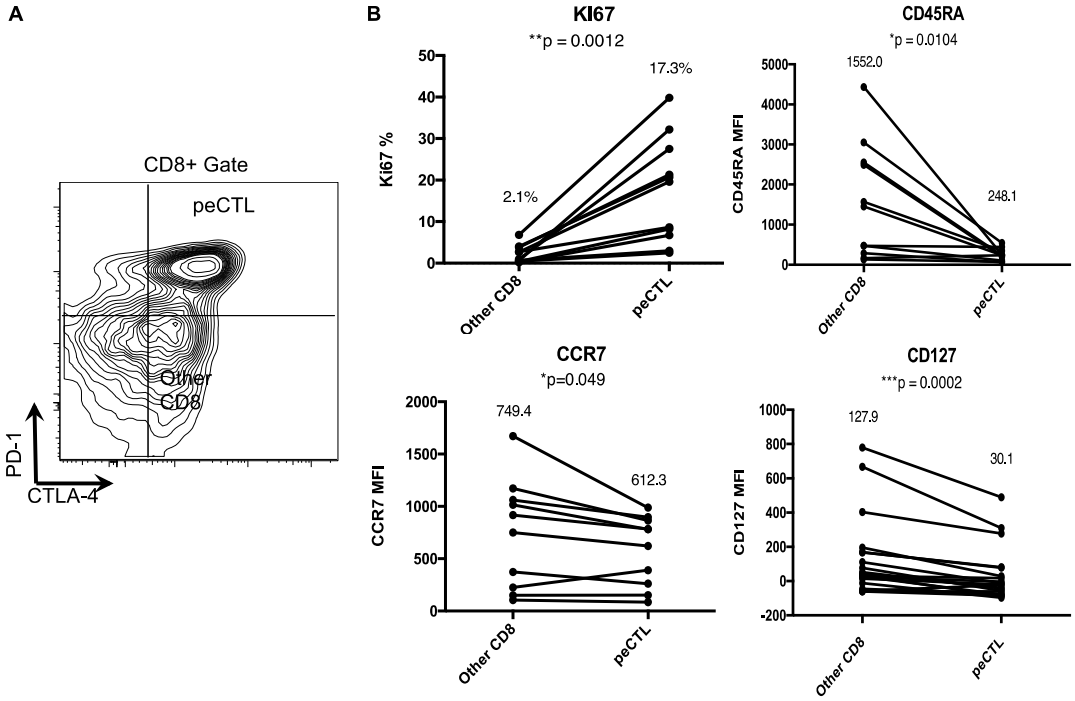

Figure 1. CTLA-4^{hi}PD-1^{hi} peCTLs have an "effector memory-like" phenotype. (A) Representative flow cytometric plot (gated on live CD45+CD3+CD8+ cells) of PD-1 and CTLA-4 expression of peCTLs from metastatic melanoma tumors (B) Flow cytometric quantification of Ki-67, CD45RA, CCR7, and CD127 expression on peCTLs and other CD8 cells within the melanoma tumor microenvironment. Each pair of connected dots represents an individual patient. MFI, mean fluorescence intensity. P values in all panels were determined by a paired, 2-tailed Student's t test.

Title: Changes in Pulmonary Autograft Wall Stresses Immediately After the Ross Procedure: First Steps Towards Understanding Autograft Dilatation

Authors: Andrew Wisneski, MD, Yue Xuan, PhD, Julius M. Guccione, PhD, Liang Ge, PhD, Elaine E. Tseng, MD.

Introduction: The Ross procedure offers treatment of congenital aortic valve disease by transplantation of the native pulmonary valve and pulmonary artery tissue, termed the autograft, into the aortic valve position. However, pulmonary autograft dilatation is the Achilles heel of the Ross procedure and often necessitates reoperation. To understand autograft remodeling, a biomechanical study of human autografts after exposure to systemic pressure is required. Our aim is to quantify wall stress on normal autografts after the Ross operation prior to dilatation. We hypothesize that elevated pressure from systemic circulation results in increased autograft wall stress which drives remodeling and dilatation.

Methods: Normal human pulmonary autografts (n=18) were acquired from human hearts rejected for transplantation from the Donor Network West. Material properties were obtained by a bi-axial stretching protocol to obtain stress-strain curves. Representative autograft geometry was provided by a previously developed human autograft model which utilized micro-computed tomography. Autograft diameter and wall stress were determined at pulmonic and systemic pressures using the computational technique of finite element analysis with LS-DYNA software.

Results: At systemic systole, mean autograft diameter was 35.56±1.68mm at the sinuses and 33.95±1.25mm at the sinotubular junction (STJ). At pulmonary systolic pressure, autograft mean diameter was 33.03±1.92mm at the sinuses and 30.97±1.36mm at the STJ. Distensibility, the percent change in diameter from diastole to systole, was 3.52% at sinotubular junction at systemic pressure and 2.60% at sinuses at systemic pressure. Peak first principal wall stress was 540±242KPa, 526±190KPa, and 583±247KPa at systemic systole in the STJ, sinuses, and annulus, respectively, compared to 90±65kPa, 88±59KPa, 96±52at pulmonic systole in the STJ, sinuses, annulus, respectively.

Conclusions: Normal human pulmonary autograft biomechanical responses to systemic pressure were quantified. A nearly 6-fold increase in peak wall stress was observed at systemic pressures. Regions of peak stress were observed in the sinuses. This data will serve as a control for future comparison to dilated pulmonary autografts, and will enable a better understanding as to which autografts may be predisposed to dilatation.

A case of two unknown primaries: concurrent metastatic p16+ oropharyngeal and cutaneous squamous cell carcinoma

Adrian E. House, MD, Chase Heaton, MD

Introduction

A 66-year-old man presented with 7 months of right-sided lagophthalmos and CN V1 (ophthalmic) neuropathy.

Methods:

Patient history, exam, imaging, pathology and chart review was used to obtain relevant information.

Results:

Imaging work-up demonstrated asymmetric enlargement and enhancement of the right supraorbital nerve, with incidental finding of a right level IIa neck mass. Fine-needle aspiration biopsy of the mass revealed p16+ SCC from a presumed oropharyngeal primary source. Supraorbital nerve biopsy also demonstrated p16+ SCC. No conclusive oropharyngeal primary was identified on scope exam and PET/CT, and skin exam did not reveal any concerning lesions. HPV DNA in situ hybridization testing was performed on both biopsy samples – the neck mass was HPV+, and the supraorbital nerve tumor HPV-. Transoral robot-assisted surgery revealed a 3mm focus of SCC within the right lingual tonsil excised with negative margins. This was followed by a neck dissection for potential single-modality treatment of his oropharyngeal SCC.

Conclusions:

After correlating imaging, immunohistochemical, and genetic testing with pathological analysis, the patient was diagnosed with two independent disease processes: p16+/HPV- cutaneous SCC metastatic to the right ophthalmic nerve, and incidentally found p16+/HPV+ T1N1M0 SCC of the right lingual tonsil metastatic to a level IIa lymph node. Thorough investigation with accurate diagnoses had major implications on cancer staging, patient prognosis, and potential treatment strategies. This case highlights the utility of HPV testing in diagnosis and management of head and neck SCC of unknown primary.

Less Is More: Cost-Effectiveness Analysis of Surveillance Strategies for Small, Nonfunctional, Radiographically Benign Adrenal Incidentalomas

Kathryn H Chomsky-Higgins[1,2], Carolyn D Seib[1], Holly M Rochefort[1], Jessica E Gosnell[1], Wen T Shen[1], James G Kahn[3], Quan-Yang Duh[1], Insoo Suh[1]

[1]Endocrine Surgery, University of California, San Francisco, [2]General Surgery, UCSF East Bay General Surgery, [3]School of Medicine, Institute for Health Policy Studies, University of California, San Francisco

Introduction: Recently published European guidelines suggest that patients with incidentally identified adrenal masses that are biochemically inactive, radiographically benign, and <4cm require neither further imaging nor biochemical evaluation. In contrast, existing United States guidelines support a regimen of surveillance after discovery of such masses. No cost-utility analysis has been performed to rigorously evaluate the relative merits of these management strategies.

Methods: We constructed a decision-analytic model to evaluate surveillance strategies for <4cm, nonfunctional, benign- appearing adrenal incidentalomas. Costs, utility values, and transition probabilities were found by literature review. The model used a societal perspective, standard 3% global discounting, and a lifetime time horizon. A strategy of no surveillance was tested against strategies of (1) one-time surveillance with noncontrast CT and standard biochemical evaluation, (2) annual surveillance for two years, and (3) annual surveillance for five years. Threshold and sensitivity analyses on key parameters were conducted to assess robustness of the model. Costs and health outcomes were represented in US dollars and quality-adjusted life-years (QALYs).

Results: In the base case, the no surveillance strategy cost $10.52 and provided 26.28 QALYs. One-time surveillance cost $105 more and provided 0.10 more QALYs for an incremental cost-effectiveness ratio (ICER) of $1052.94/QALY. All other strategies involving more surveillance were dominated; these were less effective due to loss of QALYs from false positive results of screening, exposure to radiation, and unnecessary surgery. Findings were consistent for patients younger than 40 years of age. At thresholds above 0.9% for prevalence of adrenocortical carcinoma and 16% for annual risk of progression to clinical significance for aldosteronoma, pheochromocytoma, and subclinical Cushing's syndrome, one-time surveillance was the most effective and preferred strategy. The model was robust to sensitivity analyses of disease prevalence, sensitivity and specificity of diagnostic assays and imaging, and utility estimates.

Conclusions: To our knowledge, this is the first cost-utility analysis evaluating surveillance strategies for small adrenal incidentalomas. For those patients with a <4cm, nonfunctional, benign-appearing mass, a one-time follow-up evaluation involving noncontrast CT and biochemical evaluation is cost-effective. We suggest that one-time surveillance may be a safe and potentially superior alternative to more extensive regimens.

Resolution Phenotype of Monocytes and Macrophages is Altered in Peripheral Arterial Disease

Melinda S. Schaller, Laura Menke, Mian Chen, Warren J. Gasper, S. Marlene Grenon, Michael S. Conte

Introduction: Peripheral arterial disease (PAD) is a chronic disease characterized by systemic inflammation. Monocytes (Mo) and macrophages play a central role in vascular inflammation and its resolution. We hypothesize that impaired resolution in PAD results in poor clinical outcomes.

Methods: Resolution phenotype was assessed by phagocytic activity of leukocytes, Mo cell surface markers, and cytokine profiling of Mo-derived macrophages (MDM). Phagocytosis and cell-surface markers were determined by flow cytometry. MDMs were generated from peripheral blood mononuclear cells via density gradient centrifugation. Cytokines were measured by ELISA following MDM differentiation and subsequent stimulation with LPS.

Results: Circulating Mo and neutrophils (PMN) isolated from PAD patients (n=9) demonstrated significantly lower phagocytic activity (Mo: >30%, p<.001; PMN: >25%, p<.01, Fig. 1) as compared to healthy subjects (HS) (n=14). Cell-surface marker analysis demonstrated a higher proportion of the pro-inflammatory intermediate Mo subset ($CD14^{++}16^{+}$, 1.8-fold, p=.04) in PAD compared to HS. MDM from PAD subjects retain their intrinsic inflammatory program by producing more IL-6 (PAD 3138±2676 ng/mL, HS 731±854 ng/mL p=.03) and IL-1β (PAD 244±236 ng/mL, HS 24.1±23.8 ng/mL p=.04) than those from HS. Upon stimulation with LPS, MDM from PAD subjects secrete more IL-6 (PAD 23353±22483 ng/mL, HS 5097±5836 ng/mL p=.05) than those from HS.

Conclusions: Circulating Mo and PMN in patients with PAD have substantially lower phagocytic activity as well as a greater proportion of the pro-inflammatory intermediate Mo subset compared to HS. MDM preserve their elevated inflammatory state throughout culture and retain a heightened response upon latter stimulatory cues. Collectively these data demonstrate a heightened inflammatory and impaired resolution phenotype in PAD that has potential implications for disease progression and response to interventions.

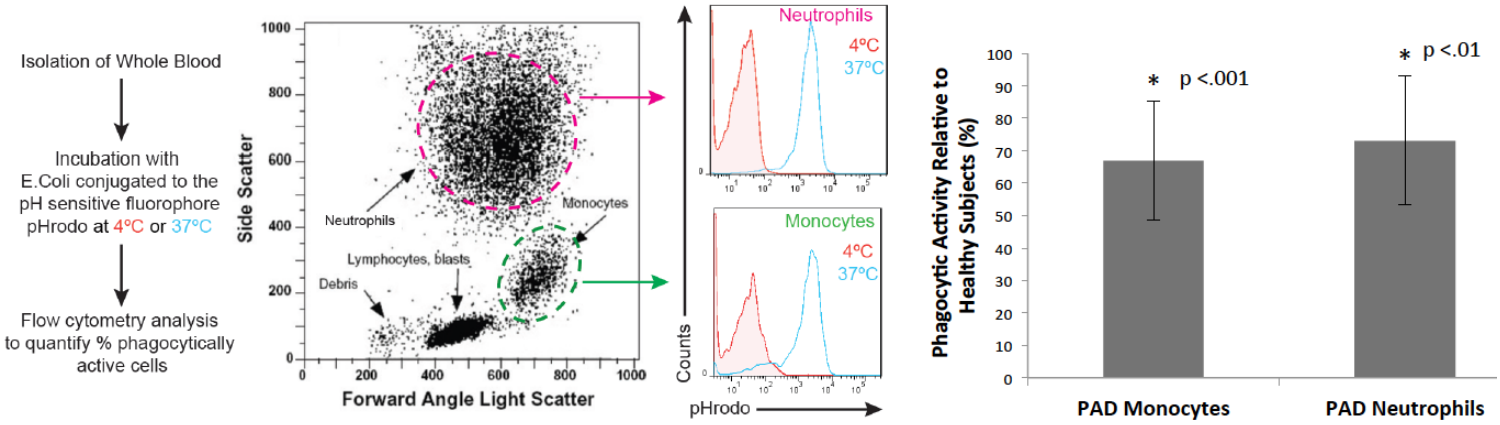

Immediate Prepectoral vs Submuscular Prosthetic Reconstruction in Nipple Sparing Mastectomy Patients: A Single Surgeon's Experience with 44 Consecutive Cases

Rachel Lentz MD, Merisa Piper MD, Monica Harbell MD, Pedram Aleshi MD, Hani Sbitany MD

Background: Nipple sparing mastectomy (NSM) with immediate reconstruction has become the gold standard for surgical management of breast cancer at our institution. Typically, prosthetic reconstruction is performed in the submuscular plane, which involves dissection and disinsertion of the pectoralis major muscle. This technique can produce significant postoperative pain and lead to breast animation deformities. Prepectoral breast reconstruction is an alternative technique that involves expander/implant placement in the prepectoral space with complete acellular dermal matrix coverage, thus eliminating the need for pectoralis muscle disruption. In this study, we compare the outcomes between immediate prepectoral and submuscular implant based breast reconstructions in NSM patients.

Methods: We retrospectively reviewed a single surgeon's experience with immediate prosthetic reconstruction following NSM from 2015-2016. Demographics, surgical and perioperative details, expansion course, and complications were compared between prepectoral and submuscular cohorts. All patients had at least 3.5 months follow up for study inclusion.

Results: We identified 44 patients who underwent 73 breast reconstructions following NSM. Twenty -two patients underwent immediate submuscular expander placement at the time of their NSM and 22 patients underwent immediate prepectoral expander placement at the time of their NSM. These groups were statistically similar with respect to age, BMI, and comorbidities. For bilateral reconstructions, total operating time was reduced an average of 23 minutes in the prepectoral cohort (240.2 vs 263.7, $p = 0.34$). Intraoperative EBL was significantly reduced (22.1 vs 28.7, $p < 0.01$). Postoperative lorazepam consumption trended nearly 30% less in our prepectoral cohort ($p = 0.31$). Initial expander fill volume (120.3 vs 104.1, $p = 0.5$) and mean number of fills to complete expansion (4.2 vs 3.9, $p = 0.54$) were similar between the two cohorts. Overall complication rates were similar between the two groups (12.5% vs 8.11%, 0.55). There were no instances of nipple necrosis/nipple loss in either group. Notably, in the submuscular cohort, the incidence of animation deformity following submuscular expander-implant exchange was 9.38%. In many of these instances, surgical correction of animation deformity, with operative conversion to prepectoral implant position, was planned to address the deformity.

Conclusions: Prepectoral prosthetic reconstruction provides a safe and patient-beneficial alternative to submuscular prosthetic reconstruction.

Therapeutic Liver Repopulation with Hepatocytes Made from Stem Cells

Hubert Luu, MD, MS; Bernadette Hsu, MS; Carlos Corvera, MD, Holger Willenbring, MD, PhD

Introduction: Many groups are working on establishing human induced pluripotent stem cells (hiPSCs) or human embryonic stem cells (hESCs) as a source of hepatocytes (hiPSC-Heps or hESC-Heps) for cell therapy of liver diseases (e.g. metabolic liver disease, acute liver failure). However, preclinical transplantation studies into FRG mice - an immune-deficient model of the human liver disease tyrosinemia type I – have shown inferior function and proliferation of hiPSC-Heps or hESC-Heps in comparison to primary human hepatocytes (PHH). One reason for this shortcoming may be that the mouse liver does not effectively promote the differentiation and proliferation of immature stem cell-derived hepatocytes. Because rats show a liver injury pattern similar to that in humans, we hypothesize that the newly developed FRG rat is more supportive of liver repopulation with hiPSC-Heps or hESC-Heps. To investigate this possibility, we are investigating the capacity of hiPSC-Heps and hESC-Heps to engraft, repopulate, and ameliorate dysfunction in the injured liver of the FRG rat.

Methods:

Primary mouse hepatocyte (PMH) isolation

To assess the principal liver repopulation capacity of FRG rats, we first transplanted primary mouse hepatocytes (PMH) into the FRG rat. Using a well-established method of hepatocyte isolation based on collagenase perfusion, PMH were acquired from a mouse liver stably expressing ZsGreen, a fluorescent protein.

Directed differentiation of hESCs into hESC-Heps

hESCs constitutively expressing GFP were cultured in feeder-free conditions on matrigel-coated plates in mTeSR1 medium. To initiate hESC-Hep differentiation, hESCs were split to a high confluency on day 0, followed by culturing for 7 days in definitive endoderm differentiation medium containing Activin A, PI-103 and CHIR99021. This was followed by culture in hepatic specification medium containing BMP4 and FGF2 for 5 days. On day 13 of differentiation, HGF was added to the culture medium, thereby generating hepatic progenitor cells by day 18. Subsequently cells were cultured in hepatocyte culture medium for 7 days to gain full maturity by day 25. Hepatocyte-like morphology was confirmed with brightfield microscopy and testing for markers of hepatocyte maturation was performed with qRT-PCR and immunofluorescence. Cells were subsequently isolated for transplantation if the maturity was confirmed.

Rat transplantation protocol

Candidate FRG rats first underwent 2/3 partial hepatectomy, followed by PMH or hESC-Heps injection into the spleen of FRG rats at either a high concentration (6-10 million) or a low concentration (1-2 million). Afterwards, the drug NTBC, which protect FRG rats from liver disease, was given in repeated cycles: absent for 7-10 days and present for 2-3 days. Liver repopulation was monitored by the presence and quantification of human albumin in rat serum by ELISA. The liver and spleen were collected at 2 or 4 weeks for histopathological analysis with direct fluorescence or immunofluorescence.

Results: Three rats undergoing transplantation with PMH recovered without complications. After 4 weeks, the livers were collected for analysis with direct fluorescence. These preliminary results demonstrated 1% engraftment by ZsGreen-labeled mouse hepatocytes in rat liver. Prior to transplantation, hESC-Heps were analyzed for SOX17, FOXA2, HNF4α, AFP, and albumin expression by qRT-PCR and immunofluorescence, which showed the expected immature hepatocyte phenotype. Two rats underwent transplantation with hESC-Heps and tolerated the procedure well. Human albumin ELISA performed at 2 weeks showed 6 ng/mL HSA, which is consistent with low-level engraftment.

Future Plans: One rat transplanted with hESC-Heps will be monitored for a total of 6-8 weeks, when the liver will be harvested for analysis with immunofluorescence for AFP, CYP3A4, and albumin. At monthly intervals, the second rat will undergo blood draw to perform HSA ELISA and assess the hESC-Hep repopulation level. Experiments will be performed in triplicate as rats become available through continued breeding.

Modeling transplant rejection and tolerance in a transgenic mouse expressing HLA-A2

Conkling, Nicole MD; Wisel, Steven MD; Ferreira, Leonardo PhD; Kaul, Anupurna PhD; Tang, Qizhi PhD

Introduction: Chronic graft rejection remains a problem of significant morbidity in the composite tissue transplant population, requiring increased doses of immunosuppression and causing often-irreversible graft injury [1]. There has been increasing interest in cellular therapies to promote tolerance, including the administration of regulatory T cells (Tregs); however, the clinical usage of polyclonal Tregs has been limited by challenges with *ex-vivo* expansion as well as lack of specificity [2, 3]. The development of chimeric antigen receptor (CAR) Tregs aims to increase the potency of administered Tregs by engineering a receptor specific to the donor tissue [4-7]. In developing our animal model utilizing CAR Tregs, we employ transgenic C57BL/6 (B6) mice that express HLA-A2. The goal of this project was to characterize the degree of cellular surface expression of HLA-A2 in various tissue types, and establish the rejection kinetics of A2-containing donor skin.

Methods: In order to examine HLA-A2 cell surface expression in the transgenic mice, animals were sacrificed and the following tissues were processed and analyzed using flow cytometry for HLA-A2 expression: skin-draining lymph nodes, spleen, blood, bone marrow, and heart. Tissues were stained with antibodies to HLA-A2, B220 (B-lymphocytes), CD4 (T-lymphocytes), and CD11c (dendritic cells). The mean fluorescence intensity (MFI) of HLA-A2 staining on various cells in each tissue type was compared to transgene-negative B6 littermate controls.

To describe the rejection kinetics of skin transplant in these mice, three transplant groups were established: complete allogeneic mismatch (B6.HLA-A2 to BALB/c), single-allele mismatch (B6.HLA-A2 to wild-type B6), and syngeneic control (transgene-negative B6 littermates to wild-type B6). The skin grafts were monitored for initial engraftment, and subsequently followed for timing of rejection.

Results: HLA-A2 expression on CD4+ lymphocytes was detected in all tissue types examined in the transgene-positive mouse, and was absent in transgene-negative littermates (Figure 1a and 1b). An identical pattern was seen for B-lymphocytes and dendritic cells. Compared with the transgene-negative littermate, mice with the HLA-A2 allele had near-universal expression in heart, peripheral blood, lymph nodes, and spleen (Figure 1c).

All skin transplants (n=15) engrafted as assessed by survival during the initial 7-day healing period prior to the onset of rejection (Figure 2 a, b, c). By day 10, both the single-allele mismatch (n=5) and allogeneic groups (n=5) showed signs of acute rejection, and the grafts were completely rejected by day 14 post-transplant (Figure 2). Syngeneic controls (n=5) displayed complete engraftment for the duration of the study (42 days).

Conclusions: The B6.HLA-A2 mouse demonstrates high surface expression in all examined tissues when compared with controls, making it an ideal source of graft tissue to test protection by anti-A2 CAR Tregs. While skin is an extremely stringent model for rejection, it is notable that single-allele mismatch skin transplant pairs exhibit identical rejection kinetics to completely allogeneic transplants. This establishes A2 as a potent antigen in the mouse model. In future experiments, rejection kinetics will be studied in solid organ and composite tissue transplant to investigate whether a higher antigenic load influences the pace and degree of rejection in this model.

References:

1. Kanitakis, J., et al., *Chronic Rejection in Human Vascularized Composite Allotransplantation (Hand and Face Recipients): An Update.* Transplantation, 2016. **100**(10): p. 2053-61.
2. Romano, M., et al., *Treg therapy in transplantation: a general overview.* Transpl Int, 2016.
3. van der Net, J.B., et al., *Regulatory T cells: first steps of clinical application in solid organ transplantation.* Transpl Int, 2016. **29**(1): p. 3-11.
4. Boardman, D.A., et al., *Expression of a Chimeric Antigen Receptor Specific for Donor HLA Class I Enhances the Potency of Human Regulatory T Cells in Preventing Human Skin Transplant Rejection.* Am J Transplant, 2016.
5. Noyan, F., et al., *Prevention of Allograft Rejection by Use of Regulatory T Cells With an MHC-Specific Chimeric Antigen Receptor.* Am J Transplant, 2016.
6. MacDonald, K.G., et al., *Alloantigen-specific regulatory T cells generated with a chimeric antigen receptor.* J Clin Invest, 2016. **126**(4): p. 1413-24.
7. Boardman, D., et al., *Antigen-specificity using chimeric antigen receptors: the future of regulatory T-cell therapy?* Biochem Soc Trans, 2016. **44**(2): p. 342-8.

Figure 1:

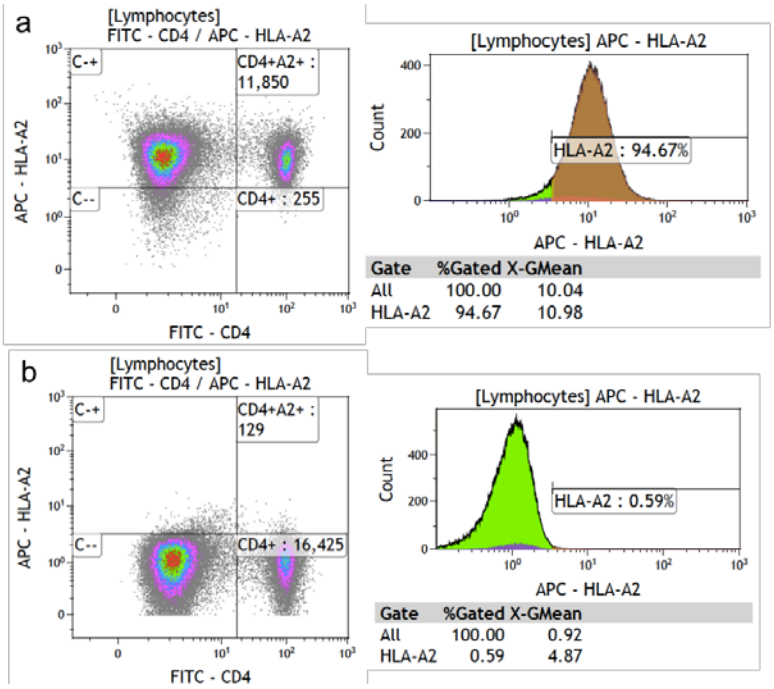

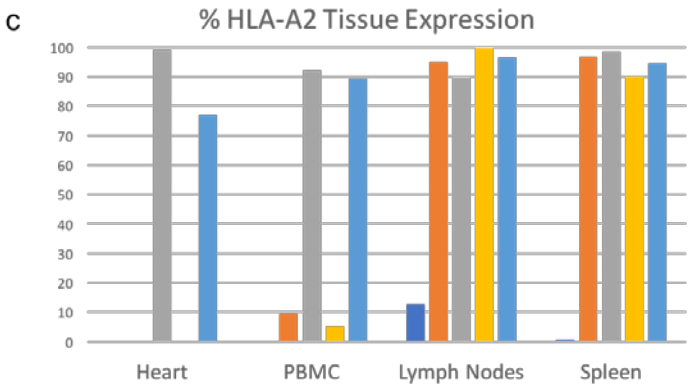

Figure 1. Measuring tissue HLA-A2 expression in transgenic mice. Mouse 52 demonstrates near-complete A2 expression on CD4+ cells in the spleen (a). In contrast, mouse 16, a transgene-negative littermate, is negative for A2 expression in this population (b). This is reflected in comparing percentage of lymphocyte populations expressing A2 in heart, peripheral blood, lymph nodes, and spleen in transgene negative (Mouse 16) with transgene positive subjects (Mice 23, 34, 48, and 52) (c).

Figure 2:

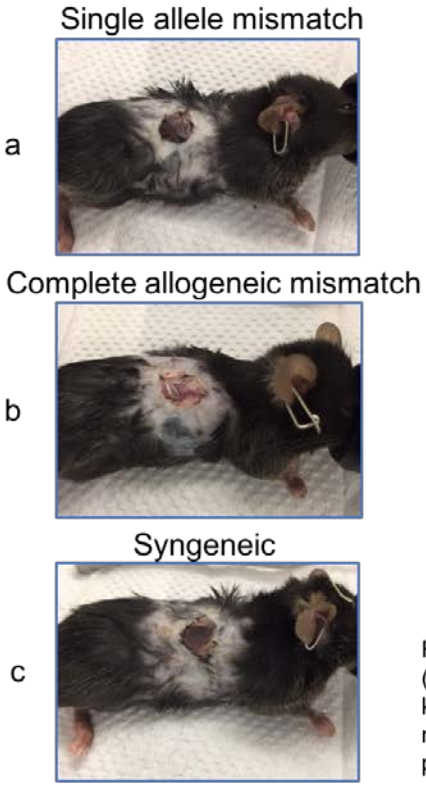

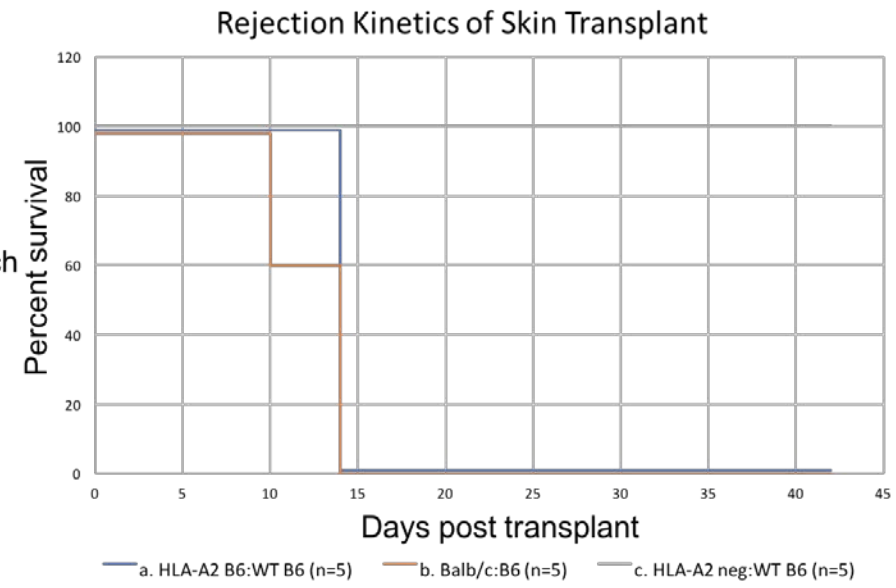

Figure 2. Skin transplant survival over time in HLA-A2-positive to wild-type B6 pairs (a), Balb/c to B6 (b), and transgene-negative littermate to wild-type B6 (c). Rejection kinetics of single-allele mismatch (a) are similar to that for complete allogeneic mismatch (b). B6 controls showed persistent engraftment for the duration of the study period.

Characterization of an Arteriovenous Mock Circulation Loop for Testing Intervascular Bioartificial Organs

Jarrett C. Moyer, M.D. – Surgery, University of California-San Francisco, San Francisco, CA;
Sukhveer S. Sandhu, M.S. – Surgery, University of California-San Francisco, San Francisco, CA;
William Fissell, M.D. – Medicine, Vanderbilt University, Nashville, TN
Shuvo Roy, Ph.D. – Bioengineering & Therapeutic Sciences, University of California-San Francisco, San Francisco, CA.

Introduction: Mock circulation loops (MCL) have been described to replicate pulmonary and systemic arterial circulation for *in vitro* testing of ventricular assist devices. Development of hemofiltration-based implantable bioartificial organs (IBO), such as the intervascular bioartificial kidney and bioartificial pancreas, relies on peripheral arteriovenous (AV) interposition for implantation and function. We developed a MCL containing pulsatile systemic arterial and non-pulsatile low pressure venous systems to replicate *in vivo* AV flow and pressure conditions for *in vitro* testing of IBO prototypes.

Methods: An AV MCL was constructed consisting of a pneumatic ventricular pump, atrial chamber, aortic and mitral swing check valves, arterial compliance chamber, arterial resistor, venous collection chamber and venous roller pump. IBO prototypes were implanted in AV fashion in an adult Yucatan pig. Systemic arterial, inflow graft, and systemic venous pressures were recorded. IBO blood flow rate was assessed using bulk flow measurement. *In vivo* pressure and flow characteristics were then compared to *in vitro* data achieved in the MCL circulating 10% glycerol through IBO prototypes.

Results: *In vivo* arterial, graft and venous pressures were 110/69 (mean 86), 78/60 (72), and 13/6 (9), respectively. The MCL yielded arterial, graft, and venous pressures of 110/67 (mean 81), 79/48 (58), and 13/10 (11). IBO blood flow *in vivo* was 1032 mL/min, compared to 940 mL/min in the MCL. The MCL was successful in replicating *in vivo* AV pressure and flow conditions through IBO prototypes. Moreover, the MCL is portable, adjustable and reusable, allowing rapid iterative *in vitro* testing of IBO prototypes. This offers device feedback and refinement of IBO design prior to expensive *in vivo* trials.

Optimization of a polycaprolactone (PCL) scaffold for islet and cellular transplantation

Steven Wisel, MD; Ryan Chang, BS; Gaetano Faleo, PhD; Peter Stock, MD, PhD; Tejal Desai, PhD; Qizhi Tang, PhD

Introduction: Islet transplantation is a proven effective therapy for patients with type 1 diabetes; however, donor shortage limits this therapy to very few patients with brittle diabetes. Stem cell therapies for beta cell replacement are quickly moving toward clinical application, but the optimal transplant site and delivery vehicle remains unknown. Previous studies have shown that three dimensional support and structure improves islet survival and function. To this end, we have optimized a polycaprolactone (PCL) polymer scaffold as a biocompatible delivery system for beta cell replacement. In these experiments, we used mouse islets as a proof-of-concept system, prior to application of the device for stem cell delivery.

Methods: PCL scaffolds of varying thickness were evaluated for maximal loading capacity *in vitro* with 150 μm PLGA fluorescent microspheres. Insulin secretion was tested *in vitro* using B6 mouse islets in a perifusion chamber (BioRep, Inc., Miami Lakes, FL). For *in vivo* testing of islet function and survival within the PCL scaffold, 200 syngeneic islets were transplanted to the epididymal fat pad of STZ-induced diabetic B6 mice, either within a PCL scaffold or directly to the epididymal fat pad. Blood glucose was measured in transplant recipient mice three times weekly for 30 days, at which point islet grafts were explanted and mice were monitored for reversion to hyperglycemia. Normal blood glucose was defined as 250mg/dL for all *in vivo* experiments.

Results: Thicker PCL scaffolds fabricated to 1.5mm thickness showed higher loading capacity compared to 1mm thick devices (383.3 versus 329 microspheres, Figure 1A). Microspheres are able to distribute within the three-dimensional porosity of the PCL scaffold, as seen by confocal microscopy (Figure 1B). Mouse islets show no limitation or delay in insulin secretion as a result of loading within the PCL scaffold on perifusion testing (data not shown). When PCL scaffolds were loaded with syngeneic islets and transplanted to the epididymal fat pad B6 mice, 3 out of 3 (100%) mice returned to normoglycemia, while 3 out of 8 (37.5%) control mice receiving free islets to the epididymal fat pad returned to normoglycemia (Figure 2). Upon explant of islet grafts from normoglycemic mice at day 30, all mice subsequently returned to hyperglycemia, confirming function of the transplanted islets.

Conclusions: Our optimized PCL scaffold supports islet survival and function in a syngeneic B6 mouse model, and may provide a delivery system for future stem cell-based beta cell replacement.

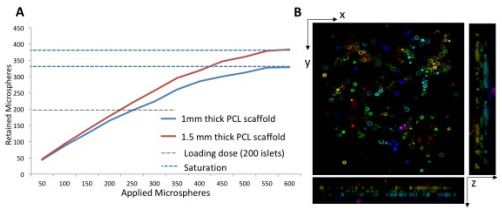

Figure 1. Characterization of PCL scaffold loading to a 3.4mm diameter prototype. A) Determination of maximal loading capacity of two PCL scaffold conformations (1.0mm and 1.5mm thickness) by application of 150 μm fluorescent PLGA microspheres. B) Confocal microscopy of PCL scaffold loaded with 150 μm fluorescent PLGA microspheres. XZ and YZ 3D projections shown at borders, with color coding for depth.

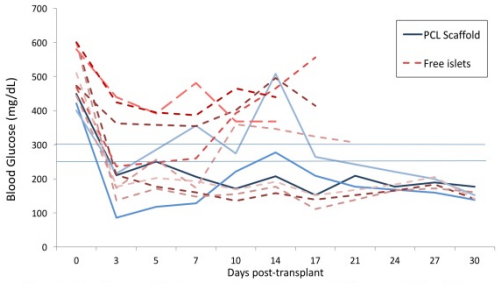

Figure 2. Blood glucose following transplant of 200 syngeneic islets to epididymal fat pad either with (PCL Scaffold, blue) or without(free islets, red) PCL Scaffold. 3/3 mice receiving PCL scaffold maintained normoglycemia until the 30 day endpoint, while 3/8 mice receiving free islets reverted to normoglycemia.

SmartDerm Automated Ulcer Risk Assessment: Real-Time Prediction and Prevention of Pressure Ulcers

Isabelle Chumfong, M.D. M.Eng.; Sharvari Deshpande, M.S.; Sachin Rangarajan, M.T.M.; Hanmin Lee, M.D.

Introduction: Pressure ulcers occur in 2.5 million patients annually, resulting in 60,000 deaths and a $30 billion burden to the healthcare system. As of 2007, neither Medicare nor Medicaid reimburses hospitals for the treatment of hospital-acquired pressure ulcers (HAPU), which can cost as much as $43,000 per treatment. Preventative measures today have limited efficacy; nurses monitor and reposition patients every two hours. These practices require significant personnel time and resources. Furthermore, the earliest visual indication of pressure ulcer formation occurs after tissue injury has already occurred. There is an unmet clinical need for a low-cost technology that can continuously monitor at-risk patients and prevent pressure ulcer formation. To meet this need, we have developed the SmartDerm system, which consists of three components: (1) a wireless network of focal pressure sensors placed on high-risk areas, (2) software that employs personalized prevention risk algorithms, and (3) decision-support software to monitor patients and suggest interventions. *We hypothesize that an individual patient's risk of developing pressure ulcers can be predicted from objective data available in the electronic health record (EHR), and that a model developed on this data can perform better at risk prediction than the current qualitative standard of care assessment, the Braden scale.* To this end, we are developing an EHR-based risk assessment algorithm, the Automated Ulcer Risk Assessment (AURA).

Methods: We have identified a cohort of n = 290 patients who developed HAPU at UCSF from 2014-2015. Variables under analysis included time since admission, type of admission, vital signs, serum chemistries, nutrition labs, serum markers of inflammation, serum markers of disease, comorbidities, and others. Statistical analysis was performed using non-parametric Wilcox rank sum testing, logistic regression, and machine learning techniques. Braden assessments were collected at the time of admission, HAPU-formation, and 12-24 hours prior.

Progress: A sub-group analysis of the first 50 patients of our cohort has been performed to test our methods. The median length of admission to development of HAPU in the subgroup was 13 days. 27% of patients in the cohort developed a pressure ulcer on their first day of admission. Non-parametric Wilcox rank sum testing was performed and revealed 13 parameters as significant predictors of ulcer development, including markers of nutrition and tissue perfusion. Additional studies are pending.

Conclusion: There is an unmet clinical need in pressure ulcer risk detection and prevention. We anticipate that AURA will allow for better prediction of HAPU risk than the current standard of care. With AURA-based decision support tools, providers will be better able to direct resources and interventions to prevent pressure ulcers and result in significant reduction in pressure ulcer incidence and cost-savings to healthcare systems.

Intraoperative Cryoanalgesia for Managing Pain After the Nuss Procedure

Claire E. Graves, Olajire Idowu, Sang Lee, Benjamin Padilla, and Sunghoon Kim

Introduction: The Nuss procedure is a common corrective operation for pectus excavatum. Unfortunately, the procedure causes significant and lengthy post-operative pain, and there is no standardized protocol for pain management. Cryoanalgesia provides long-term local nerve blockade through freezing of the intercostal nerves, leading to degeneration of the nerve axon. Because the perineurium is preserved, the axon regenerates and sensation returns in 4-6 weeks. Here, we describe a technique for thoracoscopic cryoanalgesia during the Nuss procedure and report our experience with the first 10 patients using this technique.

Methods: Cryoanalgesia of the intercostal nerves was performed prior to Nuss bar insertion through a thoracoscopic approach under direct visualization with a freezing probe (cryoICE AtriCure, Inc., West Chester, Ohio). The probe was placed at 90 degrees to the nerve and continuously treated at -60°C for 2 minutes. 5 nerves on each side were treated, lateral to the chest incision: the intercostal nerve at the level of the bar insertion, the 2 nerves above, and 2 nerves below. No epidurals were placed. A retrospective review of outcomes was performed using the electronic medical record.

Results: 8 male and 2 female patients underwent the Nuss procedure with cryoanalgesia. The mean age was 16.8 years (range 9-31 years). The mean Haller Index was 4.39 (range 3.2-8). The mean length of stay (LOS) was 2.9 days (range 2-4). Compared to the preceding 15 Nuss patients at our institution, who were treated with thoracic epidural, mean LOS was significantly shorter with cryoanalgesia (7.3 vs. 2.9 days, $P < 0.001$ via unpaired t test).

Using a verbal pain scale of 0-10, average pain on postoperative day (POD)1 was 3.44. 3 patients were discharged on POD1. Average pain score of the remaining 7 patients on POD 2 was 3.2, and of the two patients who stayed until POD3, the average pain score was 4.6. Numerical pain scores were collected for 5 patients at their 1-week postoperative day, and mean pain score was 1.1. One patient was found to have symptomatic pleural effusions at the 2-week post-operative visit, which required bilateral pigtail placement for drainage. This patient also reported stinging pain one month following the Nuss procedure, which improved with gabapentin.

Conclusion: We report a new technique of intraoperative cryoanalgesia for pain control in the Nuss procedure. The technique is easily and consistently performed under direct thoracoscopic visualization. In our first 10 cryoanalgesia patients, pain was well-controlled, and the LOS was significantly shorter than those treated with thoracic epidurals. Follow-up is planned to evaluate long-term effects. Cryoanalgesia may be the ideal strategy for pain control in Nuss patients because it is effective, durable, and reversible.

An Evidenced-Based Approach to the Identification and Treatment of Severe Acute Cholecystitis - Beyond the Tokyo Guidelines

Authors: Yvonne Kelly, MD[1], Carlos Corvera, MD[1,2], and Lygia Stewart, MD[1,2]

1 Department of Surgery, University of California San Francisco and
2 Department of Surgery, San Francisco VA Medical Center

Introduction: Acute cholecystitis (AC) variably presents from mild illness to complex disease (gangrene, abscess/perforation, Mirizzi, sepsis). The Tokyo Guidelines (TokyoG) provide guidance on treatment of severe acute cholecystitis (SevAC) but are consensus, not evidence-based. The purpose of this study was to elucidate evidence-based guidelines for the identification of SevAC and to show improvement in outcomes with the use of preoperative percutaneous cholecystostomy tube in this patient population.

Methods: We performed a retrospective review of 333 patients with acute cholecystitis. Patients were divided into two illness severity groups: 1) those with uncomplicated acute cholecystitis (AC) and 2) those with severe acute cholecystitis (SevAC). Univariate and multivariate analysis was performed to determine clinical parameters predictive of SevAC. Additionally three treatment groups were identified in the SevAC group: 1) those undergoing initial decompressive percutaneous cholecystostomy, 2) those who underwent initial surgical management and 3) those whose treatment met the previously described Tokyo guidelines (this group overlapped with the previous two). Success of laparoscopic cholecystectomy, need for additional procedures and length of stay were compared.

Results: There were 152 with AC and 181 with SevAC (47% with perforation or abscess, 40% with sepsis). The following clinical parameters were found to be significantly more prevalent in patients with SevAC: WBC > 15,000 cells/mm^3, T.bili > 1.5 mg/dl, presentation > 3 days, abscess/perforation, radiologic signs of severe inflammation, and sepsis. When ≥ 3 parameters were present, SevAC was present in 98% of cases. In contrast, Tokyo guideline definition identified SevAC in only 76% of cases. SevAC patients initially treated with a percutaneous cholecystostomy tube (C-tube) more frequently had laparoscopic cholecystectomy vs those manage by TokyoG or those managed with initial surgery (87% vs 65% vs 45%, respectively, P=0.0001); were less likely to need additional treatments (abscess drainage, re-admission, 2nd operation, etc.) (5% vs 24% vs 57%, respectively, P=0.0001); and had shorter post-op hospitalization (2 vs 5 vs 8 days, respectively, P<0.0001).

Conclusion: This study identified evidence-based clinical parameters that predicted SevAC better than Tokyo guidelines. Improved identification of SevAC and use of pre-op C-tube was associated with better outcomes than initial cholecystectomy or Tokyo guideline management (more laparoscopic procedures, fewer additional treatments, shorter post-op hospital stay).

A MICROANALYSIS OF A ROBOTIC SURGERY: INVESTIGATION INTO A SURGEON'S PROFESSIONAL VISION

Courtney A Green, MD, Hueylan Chern, MD, Ankit Sarin, MD, Patricia O'Sullivan, EdD

Without haptic feedback, robotic surgeons rely on visual processing to interpret the operative field. To provide guidance for teaching in this environment, we analyzed intracorporeal actions and language of the robotic surgeon.

The intracorporeal camera captured six hours of video during a robotic assisted lower anterior resection (LAR). Review reduced the video to 35 minutes and finally, a 2-minute clip subjected to microanalysis. The clip was replayed multiple times (capturing one, two, ten, 60 and 120 second intervals) identifying activities such as right and left hand motion, tissue handling and camera adjustments recorded using a software program. Data were synthesized into themes.

Theme 1: Changes in operative focus occurred immediately following increased activity of camera adjustment and tissue manipulation. These changes occurred after camera and tissue adjustments failed to create an operative field with appropriate tension-counter tension. Theme 2: Techniques for handling tissue highlight specific nuances in operating robotically. The surgeon manipulated tissue predominantly using blunt adjustments and rarely grasped it, likely to avoid tissue trauma. A magnified operative field required precise dissection, which occurs robotically with movement of a single instrument against a static field (motionless second robotic arm). This meticulous technique is unlike the bimodal manipulation often seen in laparoscopic dissection.

With limited active participation in robotic cases, residents rely heavily on the captured image for skill acquisition. We recommend surgeons use focus shifts as an opportunity to describe their operative decision-making and highlight instrument manipulations specific to operating with robotic technology.

Implementation of a General Surgery Registry at Soroti Regional Referral Hospital in Uganda

Yeranui Ledesma MD

Introduction: Surgical care has now been recognized as a key component of universal health coverage by the WHO, unfortunately, there is limited research on surgical outcomes in low-middle income countries, such as Uganda. The purpose of this project is to develop a sustainable surgical registry to evaluate morbidity and mortality, along with evaluation of risk factors, in post-surgical patients within a District Hospital in Uganda in order to develop quality improvement assessments.

Methods: The surgical registry will be initiated at Soroti Regional Referral Hospital, a district hospital in Eastern Uganda. A two-page paper registry tool was created after several meetings with the surgical consultants and interns. Once the registry tool was accepted, prospective data collection was initiated for patients undergoing surgery or with surgical necessity requiring transfer to another facility. All non-trauma related surgeries from general surgery, orthopedics and obstetrics-gynecology will be included in the registry. The tool will be placed in the patient's medical chart and data will be collected by surgical interns. Data will be entered into Excel and imported in STATA version 14.0 for statistical analysis.

Progress

Data collection was initiated approximately 2 weeks after arrival to Soroti Regional Referral Hospital. At this current time, all of the patients who have undergone surgery have been included for data collection. Please note at time of analysis there was a small sample size, n=40

Table 1. Patient Demographics (n=40)

Age (year) (mean, SD)	29.5	22.1
Gender (n, %)		
Male	14	35
Female	26	26
Time of Travel to Hospital (hours) (n, %)		
<1	25	69.4
1-2	5	13.9
2-4	5	13.9
>4	1	2.8
Missing	4	10.0
Length of Symptoms (n, %)		
<12 hours	1	2.5
<1 day	8	20.0
1-3 days	4	10.0
4-6 days	4	10.0
>7 days	16	40.0
>1 month	4	10.0
Missing	3	7.5
≥ 1 Comorbidity (n, %)	1	2.5
No known comorbidity (n,%)	39	97.5
Mode of Transportation (n, %)		
Motorcycle	11	27.5
Taxi	6	15.0
Private Car	1	2.5
Ambulance	1	2.5
Bicycle	1	2.5
Missing	20	50.0

Table 2. Operative Characteristics

Operation (n, %)		
Hernia Repair	3	10.7
Orthopedic	1	3.6
Suprapubic catheter	1	3.6
Small Bowel Resection	1	3.6
Soft Tissue	1	3.6
Amputation	1	3.6
Gynecologic	4	14.3
Breast	1	3.6
Cesarean	10	35.7
Colorectal	1	3.57
Degree of Urgency (n, %)		
Elective	25	62.5
Emergent	15	37.5
Type of Anesthesia (n, %)		
Spinal	18	45.0
General	6	15.0
Monitored Anesthesia	2	5.0
Local	7	17.50
Missing	7	17.50
Surgical Delays (n, %)		
None	22	55
Theater Space	3	7.5
Financial	2	5.0
Unavailable linen	2	5.0
Anesthesia	3	7.5
Surgeon	1	2.5
Sutures unavailable	3	7.5
Awaiting medication	1	2.5
Missing	3	7.5

Table 3. Multivariate logistic regression models exploring predictors for outcomes (p value), non missing values only

Outcome (n, %)	Sex	Age	Length of Symptoms	Comorbidity	Type of Operation
Mortality (2, 5.0)	0.07	0.20	0.62	<0.001	0.21
Discharged (38, 95.0)	0.07	0.20	0.62	<0.001	0.21
Surgical Complication (4, 11.4)	0.76	0.98	0.85	0.66	0.48

Conclusions: The surgical registry is the first form of documenting morbidity, mortality and potential predictors. Preliminary analysis demonstrates that the presence of comorbidities may be a predictor for morbidity and mortality in a low resource setting. One must keep in mind low sample size at this time when interpreting this data. Next steps include continuation of data collection and further analysis stratified by type of operation, age, sex, logistic regression toe valuate for independent predictors of morbidity. Ultimately, the results will be used to risk stratify preoperative patients to help guide resources and decision making. Furthermore, factors associated with morbidity and mortality will be identified for prognosis and also for development of quality improvement goals.

Title: HEALTHCARE UTILIZATION & COST OF POST-TRAUMATIC ARDS CARE

Authors: Anamaria J. Robles, Lucy Z. Kornblith, Benjamin M. Howard, Amanda S. Conroy, Ryan C. Kunitake, Carolyn M. Hendrickson, Farzad Moazed, Carolyn S. Calfee, Mitchell J. Cohen, Rachael A. Callcut

Introduction: Acute respiratory distress syndrome (ARDS) following injury has been associated with prolonged mechanical ventilation and lengthy hospitalizations. Incremental financial burden associated with increasing ARDS severity has not been previously studied. We examined cost differences of post-traumatic ARDS severity classified by Berlin criteria.

Methods: All adult highest level trauma activation patients enrolled in an ongoing prospective cohort study surviving ≥6 hours were included. For patients with PaO2:FiO2 ratio (P/F) ≤300mgHg during the first 8 days of admission, two blinded physicians reviewed chest radiographs for ARDS adjudication by Berlin criteria. Severity of ARDS was classified according to the degree of hypoxemia: mild (200<P/F≤300), moderate (100<P/F≤200), and severe (P/F≤100). Hospital charge data was utilized to perform standard costing analysis. We sought to determine the incremental cost associated with increasing ARDS severity.

Results: Adjudicated ARDS was present in 13.1% (203/1552) of patients surviving ≥6 hours. Those with ARDS were older (41 vs 35 years, p<0.01), had higher median ISS (30 vs 10, p<0.01), were more likely to have chest injury (AIS≥3: 51% vs 21%, p<0.01), and blunt mechanism of injury (85% vs 53%, p<0.01). Of the patients with ARDS, 33% had mild, 42% moderate and 25% had severe disease. There was no difference in age, mechanism, or rate of traumatic brain injury by ARDS severity. A correlation between ARDS severity and higher ISS and mortality was observed. Compared to those mild/moderate ARDS, patients with severe ARDS had increased multi-organ failure and mortality (Table). Standardized total hospital charges were four-fold higher in those with ARDS compared to no ARDS ($434K vs. $96K, p<0.01), and the highest charge per day was associated with severe ARDS (mild $20,451; moderate $23,994; severe $33,316, p<0.01).

Demographics/Outcomes by ARDS severity	Mild ARDS (n=67)	Moderate ARDS (n=86)	Severe ARDS (n=50)	*p*
Percent intubated on admission day	93%	98%	98%	<0.01
Percent transfused within 24h	64%	76%	84%	0.05
Ventilator free days	10 (0-21)	3 (0-15)	0 (0-10)	0.03
Multi-organ failure	23%	45%	58%	<0.01
ICU days	14 (7-24)	14 (8-24)	10 (4-22)	0.14
Hospital days	24 (11-51)	21 (11-42)	14 (5-25)	0.01
Total hospital charge ($)	462,417 (264,993-920,018)	489,330 (254,829-773,073)	311,017 (179,427-802,498)	0.35
Charge per day ($)	20,451 (13,398-28,133)	23,994 (14,989-32,768)	33,316 (17,175-120,735)	<0.01
Standardized total hospital charge ($)	579,528 (265,617-123,497)	495,013 (265,617-1,014,174)	338,058 (120,735-603,675)	0.01
Mortality at 28 days	21%	33%	50%	<0.01
Mortality at discharge	24%	36%	52%	<0.01

* Data are mean +/- SD, median (inter-quartile range), or n (%) as indicated. Data for skewed variables reported as median with inter-quartile ranges. Ventilator free days are counted for the first 28 days of hospitalization. Subjects who expired received 0 ventilator free days

Conclusions: The development of ARDS after traumatic injury is associated with higher healthcare costs. Among trauma patients who develop ARDS, total hospital charges per day increase with worsening severity of disease/hypoxemia. Protective strategies to prevent or mitigate ARDS after trauma are essential to controlling health care costs and should be prioritized.

Intrinsic Muscle Regenerative Capacity Following Denervation Atrophy

Alvin Wong MD, Steven Garcia, Solomon Lee, Anthony Jose, Stanley Tamaki, Jason Pomerantz MD

Introduction: Satellite cells (SCs) repair muscle following injury, reside between the basal lamina and sarcolemma, and express the transcription factor paired box protein 7 (Pax7). After injury, SCs activate, divide, migrate, and fuse with existing myofibers. SCs have been demonstrated to play a role various disease processes such as muscular dystrophy and sarcopenia. Previous studies reported SC depletion after long-term denervation, possibly explaining the irreversibility of denervation atrophy; however, these studies neither quantified nor performed functional tests on $Pax7^+$ cells specifically. Currently, it is unknown to what extent SC depletion occurs or limits recovery after denervation injury. Determining whether SCs in denervated muscle survive and retain regenerative ability in this setting will direct future approaches to muscle regeneration.

Methods: A 4mm segment of the left sciatic nerve in C57Bl6 mice was excised. To quantify SCs and their relative rate of DNA synthesis, indicators of cellular division, 3 months following denervation 100ug EdU was injected intraperitoneally for three consecutive days. Mice were sacrificed on day four and the tibialis anterior muscles (TAs) were weighed and processed for immunofluorescence analysis.

To analyze SC mitochondrial activity and gene expression, flow cytometry was used to deplete Sca-1/CD31/CD45 and select for $VCAM^+/ITGA7^+$ cells from lower leg muscles 3 and 6 months following denervation. Sorted cells were stained for Pax7 to confirm SC identity and with mitrotracker to measure mitochondrial activity. Myogenic gene expression was analyzed using quantitative reverse transcription-PCR.

To determine intrinsic regenerative capacity following denervation, SCs from 3-month uninjured and denervated legs were transplanted into the left TAs of dystrophin-deficient NSG (NSG-mdx) mice, the legs of which had been previously treated with 18 Gy radiation, to determine their ability to engraft and produce muscle fiber. Minced TA muscle grafts of C57Bl6 mice denervated for 6 months and 12 months were also implanted into the previously irradiated left TAs of NSG-mdx mice.

To assess in situ regenerative capacity, 3-month denervated C57Bl6 mice were injured with 30ul of 1.2% barium chloride ($BaCl_2$) injected into the left TA. After five days, injured TAs were analyzed for expression of MyoD, a marker of myoblast differentiation. Hematoxylin and eosin staining was performed after 30 days to assess for signs of regeneration.

Results: TAs weighed 11.9±0.6mg after 3-month denervation vs 49.5±2.5mg ($p<0.0001$). Cross-sectional fluorescent immunohistochemical staining demonstrated significant increases in the total number of $Pax7^+$ cells in denervated TAs compared to uninjured TAs (4.1±1.2 vs 1.6±0.6 $Pax7^+$ cells/100 muscle fibers, $p<0.01$) as well as in the number of sublaminar (2.9 ±0.7 vs 1.1±0.3 $Pax7^+$ cells/100 muscle fibers) and extralaminar $Pax7^+$ cells (1.2±0.5 vs 0.5±0.4, $Pax7^+$ cells/100 muscle fibers $p<0.05$). There was an increase in the total number of Edu^+ SCs in denervated TAs (0.55±0.40 vs 0.15±0.11 Edu^+Pax7^+ cells/100 muscle fibers, $p<0.05$), specifically in the extralaminar compartment (0.31±0.16 vs 0.12±0.11 Edu^+Pax7^+ cells/100 muscle fibers, $p<0.04$). In 6-month denervated TAs, the number of sublaminar SCs remained elevated (2.8±0.8 vs 2.1±0.4 $Pax7^+$ cells/100 muscle fibers, $p<0.05$), though the total number of SCs and those in the extralaminar space were not significant different.

>99% of SCs isolated from both uninjured and denervated legs expressed Pax7. SC expression levels of Pax7, MyoD, and Myf5, another marker of myoblast differentiation, were unchanged following 3 month-denervation. Satellite cells isolated from denervated legs were larger and had higher mitotracker uptake by flow cytometry at 3 and 6 months after denervation. After transplantation into the irradiated left TA of NSG-mdx mice, SCs from both uninjured and 3-month denervated leg muscles were able to produce dystrophin-expressing muscle fibers. No significant difference in the number of fibers produced by SCs from denervated and uninjured legs was noted. Minced TA muscle grafts from mice denervated for 6 and 12 months also demonstrated the ability to produce dystrophin-expressing muscle fibers after transplant into NSG-mdx mice. $BaCl_2$ injury of 3 month-denervated TAs results in a robust increase in MyoD expression on cross-sectional fluorescent immunohistochemical staining compared to the uninjured contralateral side after five days.

Conclusions: Three and six months following skeletal muscle denervation, *in vivo* SC phenotype is altered from quiescence towards activation. SCs still retain intrinsic regenerative capacity after denervation both *in situ* and following transplantation, as well as their ability to respond to chemical injury *in situ*, at least in the short term. Contrary to prior studies claiming that denervation leads to a significant decrease in the SC population over time and induces apoptosis, our results show that SCs still possess significant proliferative and regenerative capacity after long periods of denervation.

A Parsimonious Model of Mortality and Treatment Effect of Activated Protein C in Patients with Septic Shock

Barbara Hamilton, Kathleen Liu, Mark Segal, Lorraine Ware, Kirsten Johansen, Taylor Thompson, Jasleen Kukreja, Michael Matthay

Introduction. Mortality due to septic shock remains a serious concern in the critically ill. Risk prediction models such as APACHE II scoring are complex and derived using traditional methods for variable selection. Use of algorithmic methods may improve selection of baseline biologic and clinical characteristics to uncover a parsimonious risk prediction model while clarifying potential therapeutic targets. Furthermore, recent data in the critical care literature suggests that heterogeneous diseases such as sepsis may contain sub-phenotypes of patients. In a reanalysis of the Prowess-Shock trial (efficacy of activated protein C in 1696 patients with septic shock, Ranieri et al., NEJM 2012), we sought to identify a parsimonious risk prediction model for 28-day mortality. We hypothesized that a subgroup of patients at highest risk for mortality may have a different treatment effect than those not at high-risk.

Methods. Baseline data on all patients at study enrollment was extracted from the Prowess-Shock database obtained from the trial investigators. Candidate variables were initially selected using clinical judgment, then evaluated and parsed with algorithmic modeling (random forests and Lasso regression). Missing values were imputed using random forests. Independent training and testing datasets were created to analyze model predictive capability using receiving operator characteristic curves. Using a threshold probability graph and confusion matrix values, a cut-off absolute probability of mortality was chosen by which to define the high-risk group. Multivariate logistic regression was then applied to the high-risk cohort to determine the association of treatment with 28-day mortality, and the interaction between treatment and predicted mortality.

Results. Three biologic and three clinical variables independently associated with 28-day mortality were selected as the most influential and included in the model (age, protein C, lactate, creatinine clearance, plasminogen activator inhibitor 1, PaO2/FiO2 ratio) (**table**). Our six-variable model predicted 28-day mortality better than APACHE II scoring (**figure**). When a 55% predicted probability of mortality was applied to define the high-risk group, treatment with active protein C was found to decrease mortality by more than two-fold (**table**). In the high-risk group, an interaction was found between treatment and predicted mortality ($p=0.021$).

Conclusions. Using algorithmic modeling of a large cohort of patients in septic shock, we have identified a parsimonious risk-prediction model that provides better predictive capabilities than conventional methods such as APACHE II scoring. We used this model to uncover a sub-phenotype of high-risk patients that may benefit from treatment with activated protein C.

Table. Association of baseline characteristics with 28-day mortality.

	OR	95% CI	p-value
Treatment (entire cohort)	0.946	(0.713 , 1.253)	0.697
PAI-1 (ln)	1.277	(1.132 , 1.442)	0.000
Protein C (ln)	0.681	(0.537 , 0.865)	0.002
Lactate (ln)	1.333	(1.039 , 1.717)	0.025
Age (10 years)	1.395	(1.248 , 1.564)	0.000
Creatinine clearance (20 mL/min)	0.893	(0.810 , 0.975)	0.017
PaO2/FiO2 ratio (increments of 50)	0.830	(0.768 , 0.894)	0.000
Treatment* (high-risk only)	0.338	(0.111 , 0.957)	0.047

OR, odds ratio; CI, confidence interval; PAI-1, plasminogen activator inhibitor 1.
**Interaction term of treatment with predicted mortality: 0.282, p=0.021.*

Figure.

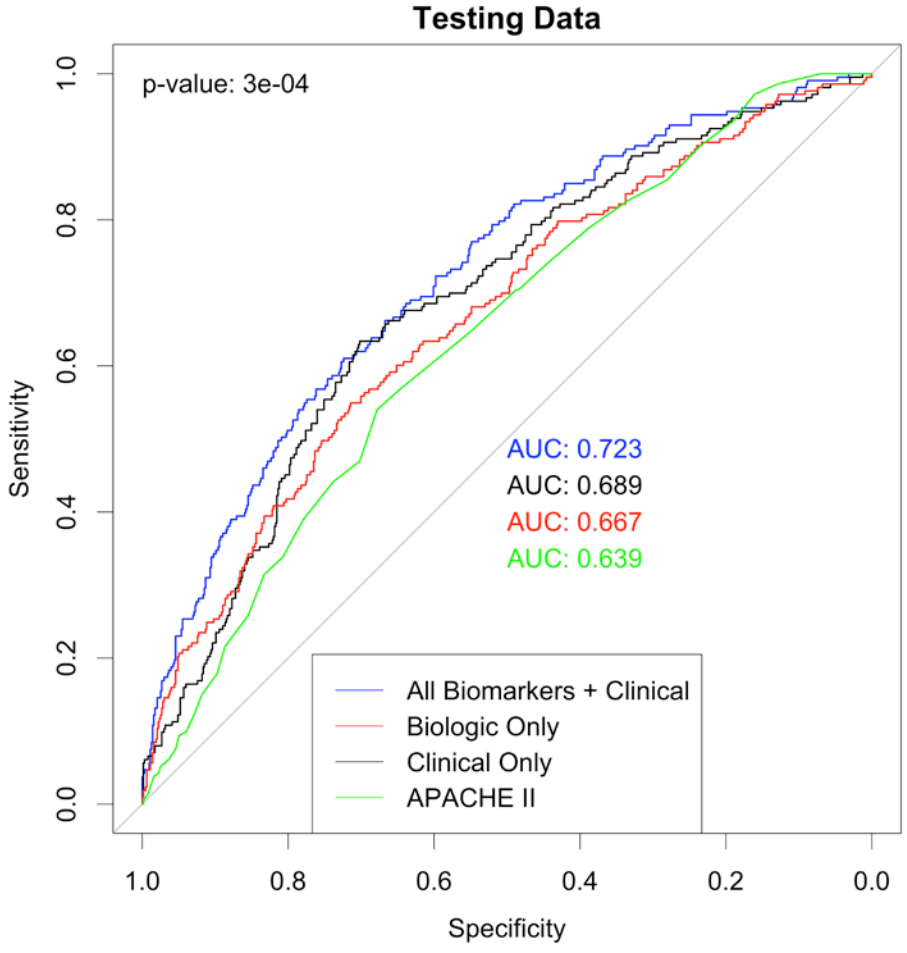

INJURY AND CARE-SEEKING IN SOUTHWEST CAMEROON: A COMMUNITY BASED SURVEY

Christie SA, Dickson DC, Nana T, Stern PMO, Chichom-Mefire A, Dicker RA, Juillard C

Introduction: Trauma is a leading cause of death in low and middle-income countries (LMIC). Existing data are predominantly derived from hospital registries that exclude persons who do not present to formal care. This selection bias likely underreports the impact of injury overall, but particularly among vulnerable populations who may be less likely to access formal care. To characterize potential targets for access expansion, we conducted a regional community based survey with the aim of identifying yearly incidence and epidemiology of injury, as well as determinants of formal care-seeking in the Southwest Region of Cameroon. We present here the preliminary findings of data collected from our first 11 enumeration areas.

Methods: Three-stage cluster sampling with probability proportionate to population was used to select 36 enumeration areas in Southwest Cameroon. Household representatives at each site were asked to describe all injuries occurring in the preceding 12 months that resulted in death, loss of routine daily activity, or required medical attention. Data on injury type, care-seeking behavior, cost of treatment, disability and economic impact were collected. Selected families reporting recent injury were targeted for semi-structured qualitative interviews to explore perceptions and values underlying care-seeking choices.

Results: Among 2586 individuals surveyed in 11 enumeration areas in Southwest Cameroon, 6.00% (95CI 4.4-8.2%, DEFF 0.81) of respondents had been injured in the past year. There were a total of 165 injury events for an overall injury incidence of 64 injuries/1000 person-years (95CI 55-75/1000 person-years). Incidence of fatal injury was 1.55/1000 person-years (95CI 0.58-4.1/1000 person-years). Approximately 33%(SE 4.41) of injuries causing disruption of daily activities never received formal medical care services and a further 10% (SE 2.34) of injuries had delayed presentation to formal care. Road traffic incident (RTI) was the most common injury mechanism both overall (35%) and among severe injuries (45%) and 70% of RTIs involved commercial vehicles. Upper and lower extremity injuries were most frequently reported (61% and 24% of injuries), followed by head and neck injury (17%). Approximately 8.3% of injuries resulted in loss of consciousness at the scene. The injuries described in this cohort led to 1573 disability days/1000 person-years and 29.9%(SE 4.22) reported ongoing disability at the time of the survey. Eighteen percent of injuries (SE 4.22) resulted in the injured person losing their job or stopping school after injury. Estimated treatment costs were significantly greater for those who presented to formal care (73.87 USD vs. 18.96 USD, p-value <0.001). Forty-one percent of injuries (SE 4.9) required the household to sell assets, borrow money, or liquidate savings to pay for medical treatment and 32% (SE 5.7) resulted in economic hardship severe enough to cause difficulty in paying for basic necessities such as food and housing. Preliminary analysis of qualitative data suggests that perception of injury severity plays a critical role in determining care-seeking behavior and is frequently assessed based on mechanism-type rather than symptoms. Anticipated cost and cost-structure, ease of access, and perceived carelessness or corruption at hospitals form major barriers to formal health care usage.

Conclusions: Injury occurs commonly in Southwest Cameroon and results in considerable physical and economic disability. Up to 40% of injured persons do not present to formal medical care or present after seeking another care source. Critical determinants of care-seeking include affordability, concerns regarding hospital carelessness, and perceptions of injury severity. The degree of economic hardship incurred by injured individuals and the associated reluctance to seek care for fear of economic repercussions should prompt investigation into health financing schemes for trauma and other emergencies. Resources should be mobilized to prioritize injury prevention and increase acceptability of formal medical services to improve outcomes after injury.

TABLE 1: Cost of Treatment and Indicators of Economic Disibility by Formal Care Utilization After Injury in Southwest Cameroon	No Formal Care		Formal Care Sought		
	Mean / %	Std. Err.	Mean / %	Std. Err.	*p-value*
Estimated Cost of Medical Care (USD)	73.87	12.83	18.96	19.50	*<0.001*
Households with New Difficulty Affording Neccessities (%)	23.4%	7.6%	37.1%	6.6%	*0.18*
Household Borrowed Money or Sold Assets (%)	22.9%	7.5%	50.5%	5.9%	*<0.001*